Revisiting the Role of the Water Vapor and Lapse Rate Feedbacks in the Arctic Amplification of Climate Change

EMMA BEER[a] AND IAN EISENMAN[a]

[a] *Scripps Institution of Oceanography, University of California San Diego, San Diego, California*

(Manuscript received 19 October 2021, in final form 13 January 2022)

ABSTRACT: The processes that contribute to the Arctic amplification of global surface warming are often described in the context of climate feedbacks. Previous studies have used a traditional feedback analysis framework to partition the regional surface warming into contributions from each feedback process. However, this partitioning can be complicated by interactions in the climate system. Here we focus instead on the physically intuitive approach of inactivating individual feedback processes during forced warming and evaluating the resulting change in the surface temperature field. We investigate this using a moist energy balance model with spatially varying feedbacks that are specified from comprehensive climate model results. We find that when warming is attributed to each feedback process by comparing how the climate would change if the process were not active, the water vapor feedback is the primary reason that the Arctic region warms more than the tropics, and the lapse rate feedback has a neutral effect on Arctic amplification by cooling the Arctic and the tropics by approximately equivalent amounts. These results are strikingly different from previous feedback analyses, which identified the lapse rate feedback as the largest contributor to Arctic amplification, with the water vapor feedback being the main opposing factor by warming the tropics more than the Arctic region. This highlights the importance of comparing different approaches of analyzing how feedbacks contribute to warming in order to build a better understanding of how feedbacks influence climate changes.

KEYWORDS: Arctic; Feedback; Water vapor

1. Introduction

The Arctic is warming at a faster rate than lower latitudes, in a phenomenon known as Arctic amplification, and it is projected to continue to do so in the future (e.g., Collins et al. 2013). Climate feedback processes play an important role in Arctic amplification, and different feedbacks have been variously proposed to be the main drivers (e.g., Hall 2004; Screen and Simmonds 2010; Taylor et al. 2013; Pithan and Mauritsen 2014; Goosse et al. 2018; Stuecker et al. 2018). These include latitudinal variations in the Planck feedback, since the Planck feedback is a weaker negative feedback in the polar regions; the lapse rate feedback, which accounts for vertical variations in warming in the atmosphere; and the surface albedo feedback (SAF), which occurs due to the loss of snow and sea ice causing a change in absorbed solar radiation and has traditionally been thought to play a key role in Arctic amplification. Other climate processes that have also been proposed to play a role in Arctic amplification include the water vapor feedback, since a warmer atmosphere can hold more water vapor (which is a greenhouse gas), as well as cloud feedbacks and poleward heat transport in both the atmosphere and ocean (e.g., Holland and Bitz 2003; Alexeev et al. 2005; Francis and Hunter 2006; Kay and Gettelman 2009; Hwang et al. 2011; Mahlstein and Knutti 2011; Alexeev and Jackson 2013; Goosse et al. 2018; Beer et al. 2020).

Studies of Arctic amplification are hampered by the complexity of the climate system, making it challenging to quantify the effects of a single process. One metric that has been used in many studies of climate change is radiative forcing, which measures the net change in Earth's energy balance and allows a relatively simple method for comparing the climate response to different forcings and feedbacks (Myhre et al. 2013). A typical form of analysis using radiative forcing borrows the feedback framework from electrical engineering and relates perturbations of top-of-the-atmosphere (TOA), or alternately tropopause, radiative forcing to changes in the global-mean surface temperature (see Fig. A1 in appendix A). A traditional feedback analysis is then used to attribute warming caused by each feedback by partitioning the total change in global-mean surface temperature into individual contributions from feedbacks and other processes (e.g., Dufresne and Bony 2008).

More recently, this traditional feedback analysis framework has been extended to look at regional warming due to local values of spatially varying feedbacks (e.g., Armour et al. 2013), and a number of studies have investigated the contribution of each climate feedback to Arctic amplification. Using this method, the lapse rate feedback has been identified to contribute the most to Arctic amplification, followed by variations in the Planck feedback and the SAF (Pithan and Mauritsen 2014; Stuecker et al. 2018; Goosse et al. 2018). The water vapor feedback, while being a positive feedback everywhere, is strongest in low latitudes and is found to contribute more to tropical warming than Arctic warming, making it the largest factor opposing Arctic amplification according to these analyses. Studying local warming by using such an analysis of the regional structure of feedbacks is relatively computationally efficient and allows for a clean decomposition of the

Corresponding author: Emma Beer, ebeer@ucsd.edu

DOI: 10.1175/JCLI-D-21-0814.1

surface warming, because the sum of the warming contributions of individual feedbacks is equal to the total warming. However, it does not consider changes in atmospheric heat transport (AHT) associated with the strength of individual feedbacks, which affects local warming and can have an influence on Arctic amplification (e.g., Langen et al. 2012; Merlis 2014; Russotto and Biasutti 2020). Therefore, one might argue that the traditional feedback analysis framework does not have a clear physical interpretation for the attribution of Arctic amplification.

Another method that has been used to assess the influence of specific climate feedbacks in some studies is feedback locking. Warming can be attributed to an individual feedback in this method by "locking" a feedback in a model and looking at the change in forced warming when the feedback does not act on the perturbation to the climate system. For example, studies that locked the surface albedo feedback have found it has a large impact on polar amplification (Hall 2004) but a smaller impact on the global mean temperature (Graversen and Wang 2009). By locking cloud feedbacks, it has been found that global cloud radiative feedbacks have a warming effect on the Arctic, but both global and local Arctic cloud radiative feedbacks have little influence on Arctic amplification (Middlemas et al. 2020). Studies that lock climate feedbacks have also found that AHT can compensate for feedbacks being inactivated, causing the warming response to be similar to when all feedbacks are included (Langen et al. 2012). AHT has similarly been found to compensate for latitudinal differences in climate feedbacks, causing feedbacks to have similar contributions to warming both the tropical and polar regions (Russotto and Biasutti 2020). A benefit of this method is that perturbing the strength of a feedback in a model allows for other feedbacks and processes to adjust to changes in the perturbed feedback. On the other hand, a drawback when this method is applied to the full set of climate feedbacks is that the warmings attributed to individual feedbacks do not sum up to the total amount of warming due to feedback interactions (as discussed in section 4 below).

Feedback locking experiments in comprehensive climate models are computationally expensive, and previous studies have typically focused on locking a single feedback process. A moist energy balance model (MEBM), which approximates AHT as a diffusive process that involves both surface temperature and specific humidity, is more computationally efficient. Although idealized, MEBMs have been shown to capture the changes in temperature and AHT simulated in comprehensive climate models (Bonan et al. 2018; Armour et al. 2019), and many studies have demonstrated that they can be a useful tool to assess the impact of individual radiative feedbacks on changes in temperature and AHT under global warming (Hwang and Frierson 2010; Hwang et al. 2011; Rose et al. 2014; Roe et al. 2015; Bonan et al. 2018; Russotto and Biasutti 2020).

In this study, we evaluate the individual contributions of all radiative climate feedbacks to Arctic amplification using a suite of feedback locking simulations with a MEBM, and we compare this with the results of a traditional feedback analysis. Determining how much each feedback contributes to Arctic amplification depends on how a feedback contribution is defined. We contrast the two methods and quantify how the warming anomaly associated with a given feedback causes further warming anomalies associated with each of the other feedbacks and AHT. These effects cause differences between warming contributions in the traditional feedback analysis and the warming attributed to each feedback in our feedback locking analysis. We specify feedbacks from phase 5 of the Coupled Model Intercomparison Project (CMIP5; Taylor et al. 2012), allowing a direct comparison with previous studies that used traditional feedback analyses (Pithan and Mauritsen 2014; Goosse et al. 2018).

2. Attributing warming to individual feedbacks

We use a moist energy feedback model, which solves for the change in surface temperature under heating that includes both specified forcing and simulated changes in AHT. For the feedback locking analysis, we lock individual climate feedbacks in the MEBM, while allowing everything else to evolve. By taking the difference in surface warming between the simulation with all feedbacks active and the simulation with an individual feedback locked, we calculate the warming associated with the locked feedback. This approach accounts for feedback interactions in that the additional warming that arises when a feedback is included is modulated by the other feedbacks and AHT (see details in section 4). We compare the warming calculated from the locking analysis to warming contributions from a traditional feedback analysis.

For both analyses, we use spatially varying climate feedback parameter values diagnosed from CMIP5 global climate model (GCM) simulations (see appendix B for details regarding the calculation of feedback parameter values). Each climate feedback parameter has a meridional structure, $\lambda_i(\phi)$, where ϕ is the latitude. The sum of the individual feedbacks is the total feedback parameter:

$$\lambda(\phi) = \lambda_0 + \sum_i \lambda_i(\phi), \tag{1}$$

where the Planck feedback has been divided into a global-mean value λ_0 and latitudinally varying departures from this, which is one of the terms λ_i, with i being the index of the individual feedback. Note that when we refer to the index associated with a specific feedback, we will insert for i an abbreviation for the name of the feedback rather than a number (e.g., λ_{LR} for the lapse rate feedback parameter).

The TOA energy budget, which relates changes in surface temperature $T(\phi)$ to changes in heating $F(\phi)$, can be written as

$$0 = \lambda(\phi)T(\phi) + F(\phi). \tag{2}$$

The heating can be broken down into perturbations to the radiative forcing (e.g., from rising greenhouse gas concentrations) F_{RAD}; changes in ocean heat uptake and transport, diagnosed as the anomalous net surface heat flux F_{OHU}; and changes in AHT convergence in the atmospheric column F_{AHT}:

$$F(\phi) = \underbrace{F_{\mathrm{RAD}}(\phi)}_{\substack{\text{perturbation to}\\ \text{radiative forcing}}} + \underbrace{F_{\mathrm{OHU}}(\phi)}_{\substack{\text{change in ocean}\\ \text{heat uptake}}} + \underbrace{F_{\mathrm{AHT}}(\phi)}_{\substack{\text{change in atmospheric}\\ \text{heat transport}}}. \quad (3)$$

Values of F_{RAD} and F_{OHU} are diagnosed from CMIP5 (see appendix B) as functions of latitude, similar to the feedback parameters λ_i. The perturbations in surface temperature T and AHT F_{AHT} are computed with the MEBM. The computed T and F_{AHT} fields in the MEBM simulation with all feedbacks active are used in the traditional feedback analysis.

a. Moist energy balance model

MEBMs are based on the dry energy balance model (EBM) framework (Budyko 1969; Sellers 1969) but add the latent heat effects of atmospheric moisture transport, which allows them to more accurately portray AHT (Hwang and Frierson 2010). Here we use an MEBM that was developed and evaluated in previous studies (Roe et al. 2015; Siler et al. 2018; Bonan et al. 2018; Armour et al. 2019).

We use a perturbation form of the MEBM that solves for the climate response to a change in forcing, with the values of λ_0, $\lambda_i(\phi)$, $F_{\mathrm{RAD}}(\phi)$, and $F_{\mathrm{OHU}}(\phi)$ specified based on CMIP5 output. The MEBM approximates AHT as the diffusion of moist state energy (MSE) h, taking into account converging meridians on Earth and using a constant diffusion coefficient $D = 2.61 \times 10^{-4}$ kg m^{-2} s^{-1} [consistent with the diffusivity value of 1.06×10^{6} m^2 s^{-1} used in Hwang and Frierson (2010)] to give the perturbation in AHT as

$$F_{\mathrm{AHT}}(\phi) = D\,\frac{d}{dx}\left[(1-x^2)\frac{dh(\phi)}{dx}\right], \quad (4)$$

where $x \equiv \sin\phi$ and the MSE perturbation is

$$h(\phi) \equiv c_p T(\phi) + L_v q(\phi). \quad (5)$$

Here, $c_p = 1004$ J kg^{-1} K^{-1} is the specific heat of air and $L_v = 2.45 \times 10^{6}$ J kg^{-1} is the latent heat of vaporization. The anomalous specific humidity q is calculated using the Clausius–Clapeyron relation, which approximately relates water vapor pressure to temperature:

$$q(\phi) = \frac{\epsilon r e_0}{p}\left(\exp\left\{\frac{a\left[T_0(\phi)+T(\phi)\right]}{b+T_0(\phi)+T(\phi)}\right\} - \exp\left[\frac{aT_0(\phi)}{b+T_0(\phi)}\right]\right), \quad (6)$$

where $\epsilon = 0.622$ is the moisture constant, $e_0 = 611.2$ Pa is the vapor pressure, $p = 9.8 \times 10^{4}$ Pa is the surface pressure, $a = 17.67$ and $b = 243.5$ K are the saturation vapor constants, and T_0 is the mean state temperature expressed as the departure from 273.15 K, which is estimated from the ERA-Interim reanalysis (Dee et al. 2011) as a function of latitude. As in previous studies, we keep the relative humidity fixed at a value of $r = 0.80$ in the calculation of MSE (e.g., Hwang and Frierson 2010; Roe et al. 2015; Siler et al. 2018), so we are only including changes in specific humidity due to changes in temperature. This allows the MSE h to be written as a function of only the surface temperature T simulated in the MEBM and specified model parameters.

This MEBM configuration is adopted from Bonan et al. (2018), who found that the MEBM can account for 90% of the variance in surface temperature in the CMIP5 GCMs.

b. Traditional feedback analysis

We begin by considering a traditional feedback analysis of the warming contributions associated with the regional structure of feedbacks. First, Eqs. (1) and (2) are rearranged as

$$T(\phi) = \frac{F(\phi)}{-\lambda_0} + \sum_i \lambda_i(\phi)\,\frac{T(\phi)}{-\lambda_0}. \quad (7)$$

Equation (7) is illustrated schematically in Fig. A1 in appendix A. The first term represents warming in the absence of any feedbacks, and it can be readily split into warming contributions from F_{RAD}, F_{OHU}, and F_{AHT}. The second term represents the sum of the warming contributions from each feedback T_{i*}, which are defined as

$$T_{i*}(\phi) \equiv \lambda_i(\phi)\frac{T(\phi)}{-\lambda_0}. \quad (8)$$

The feedback parameters and warming contributions based on this traditional feedback analysis are plotted in Figs. 1a–d.

c. Feedback locking analysis

To examine the amount of warming that would occur in the absence of a given feedback process, we run a simulation with the MEBM in which an individual feedback parameter field is subtracted from the total feedback parameter. Since the MEBM we are using is a model of anomalies from the reference climate, turning off a specific feedback is equivalent to keeping the climate fields associated with the feedback locked at the climatological state. Hence, we refer to this approach as "feedback locking," a term used to describe similar experiments in previous studies (e.g., Graversen and Wang 2009; Langen et al. 2012; Middlemas et al. 2020). Note that these types of experiments are sometimes described in the literature with other terminology, including "suppressing" feedbacks or "turning off" feedbacks. An example of feedback locking is fixing the surface albedo at its climatological value. This form of feedback locking has been used in previous studies to look at effects of the surface albedo feedback on local and nonlocal warming, polar and global warming, and internal variability (Cess et al. 1991; Hall 2004; Graversen and Wang 2009; Roe et al. 2015).

In the MEBM, a feedback is locked by replacing $\lambda(\phi)$ with $\lambda(\phi) - \lambda_i(\phi)$. We refer to the resulting warming simulated by the MEBM as T_{-i}. Since the different temperature perturbation causes a different simulated F_{AHT}, we refer to the resulting heating as F_{-i}. We can then write the perturbation equation for the MEBM [Eq. (2)] when a feedback is locked as

$$0 = \left[\lambda(\phi) - \lambda_i(\phi)\right]T_{-i}(\phi) + F_{-i}(\phi). \quad (9)$$

We calculate the warming attributed to each feedback process in this approach T_i as the difference between the result

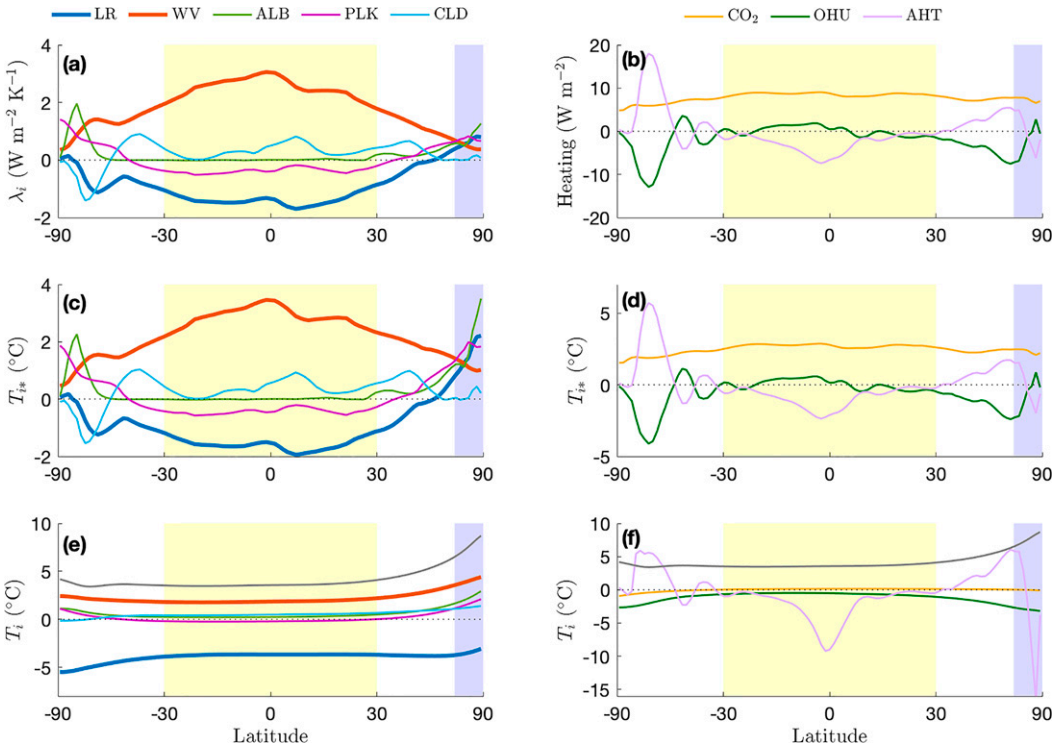

FIG. 1. Latitudinally varying variables as calculated from CMIP5 simulations and MEBM simulations. (top) Feedbacks and heating terms diagnosed from CMIP5 simulations. (a) Feedback parameters (λ_i) for each radiative feedback process: lapse rate (LR), water vapor (WV), surface albedo (ALB), Planck deviation from global-mean value (PLK), and cloud (CLD). (b) Heating terms: CO_2 forcing (CO_2), changes in ocean heat uptake (OHU), and changes in atmospheric heat transport (AHT). (middle) Warming contributions from each feedback process based on a traditional feedback analysis (T_{i*}). (c) Warming contributions for each feedback, which are proportional to the product of the feedback parameter [in (a)] and the total temperature change. (d) Warming contributions for each heating term, which are proportional to the heating term [see (b)]. (bottom) Results of the feedback locking analysis (T_i). (e) Warming for each radiative feedback. (f) Warming for each heating term: deviation from global mean CO_2 forcing (CO_2), changes in ocean heat uptake (OHU), and changes in atmospheric heat transport (AHT). In all panels, yellow and blue shading represent the tropical and Arctic regions, respectively. This study focuses on the LR and WV feedbacks, which are indicated by thicker lines in (a), (c), and (e). The horizontal axes are scaled to be uniform in $x \equiv \sin(\text{latitude})$; note that each increment of x is proportional to the surface area of the associated latitude band.

with all feedbacks active T and the result with the individual feedback locked T_{-i}:

$$T_i(\phi) \equiv T(\phi) - T_{-i}(\phi). \tag{10}$$

For the warming associated with the latitudinal variations in the CO_2 forcing, in the locked simulation we set F_{RAD} to its global-mean value. We set $F_{\text{OHU}} = 0$ or $F_{\text{AHT}} = 0$ in the locked simulations for the warming associated with changes in ocean heat uptake or changes in AHT. The warming attributed to each feedback and to each heating term using feedback locking in the MEBM is shown in Figs. 1e and 1f.

3. Lapse rate and water vapor feedbacks

In both the feedback locking analysis and the traditional feedback analysis, we average the warming associated with each feedback over the Arctic region (60°–90°N) and the tropical region (30°S–30°N) in order to quantify the contributions to Arctic amplification (Fig. 2). The results show striking differences between the two approaches, especially for the water vapor and lapse rate feedbacks, which we focus on for the remainder of this study. The water vapor feedback is the largest factor opposing Arctic amplification in the traditional feedback analysis (i.e., it is the point farthest in the downward right direction from the dashed line in Fig. 2a). In the feedback locking analysis, by contrast, it is the largest contributor to Arctic amplification (the point farthest in the upward left direction from the dashed line in Fig. 2b). The lapse rate feedback is the largest contributor to Arctic amplification in the traditional feedback analysis (Fig. 2a), warming the Arctic while cooling the tropics. By contrast, it has an approximately neutral effect in the feedback locking analysis (Fig. 2b), because it cools the tropics and the Arctic by similar amounts.

These differences between the results of the two analyses in Fig. 2 highlight the importance for each feedback process of interactions with other feedback processes and with the

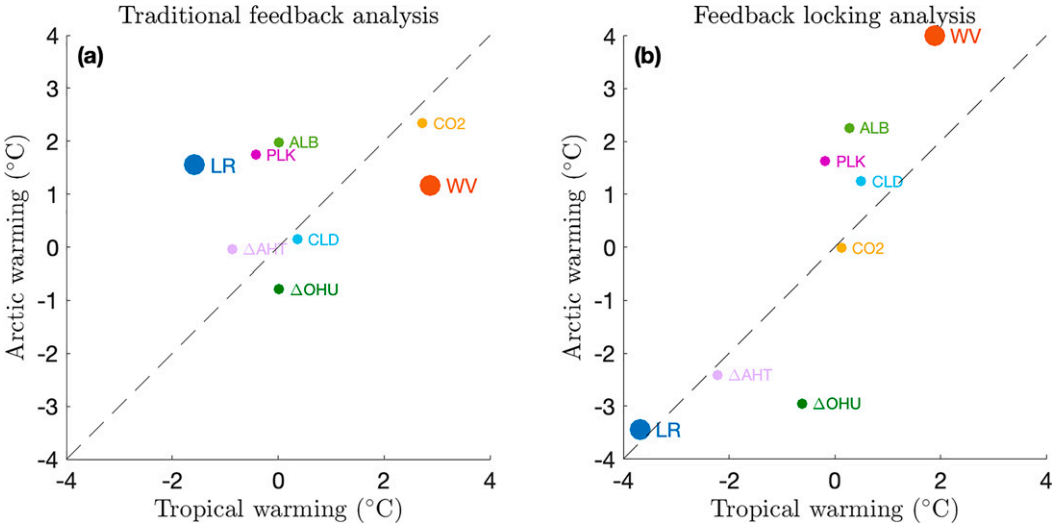

FIG. 2. Contributions of each feedback process and heating term to Arctic amplification, plotted as Arctic warming vs tropical warming. (a) Warming contributions calculated using a traditional feedback analysis [Eq. (7)], as used in previous studies. (b) Results of the feedback locking analysis [Eq. (10)], which is suggested here to be a physically intuitive approach. Here the lapse rate feedback (LR), water vapor feedback (WV), surface albedo feedback (ALB), Planck feedback deviation from the global-mean value (PLK), cloud feedbacks (CLD), CO_2 forcing (CO_2), changes in ocean heat uptake (ΔOHU), and changes in atmospheric heat transport (ΔAHT) are plotted. Note that in the traditional feedback analysis, CO_2 forcing includes both the global mean and the spatially varied deviation, whereas in the feedback locking analysis, CO_2 forcing is taken as the deviation from the global-mean value. Tropical warming is averaged over 30°S–30°N, and Arctic warming is averaged over 60°–90°N. The LR and WV feedbacks, which are the focus of this study, are indicated by larger circles.

meridional energy transport. The water vapor feedback parameter is positive everywhere, but it is considerably larger in the tropical region than in the Arctic (Fig. 1a). Warming contributions in the traditional feedback analysis scale as the feedback parameter (Fig. 1a) times the total warming (gray line in Figs. 1e,f). Although the warming is greater in the Arctic than in the tropics, this difference is not sufficient to overcome the difference in the feedback parameter, and the result is that the warming contribution from water vapor is larger in the tropics than in the Arctic (Figs. 1c and 2a).

However, things change when the climate system is allowed to respond to the omission of the water vapor feedback. Removing the concentrated warming in the tropical region caused by the water vapor feedback leads to a decrease in the temperature gradient between the equator and the pole, and hence a decrease in the meridional transport of MSE in the MEBM. This is most evident in Fig. 3a in the equatorial region, where there is increased heating by AHT when the water vapor feedback is suppressed. A smaller level of decreased heating in the polar region can also be seen in Fig. 3a. In other words, the inclusion of the water vapor feedback causes AHT to cool the tropics and warm the Arctic.

There are also interactions between the water vapor feedback and other feedbacks in the MEBM; that is, other feedbacks react to the change in warming due to the inclusion or omission of the water vapor feedback. When the water vapor feedback is locked, the total feedback felt by the model ($\lambda - \lambda_{WV}$) is less negative in the Arctic region than in the tropical region (Fig. 3b). Therefore, because water vapor is a positive feedback, it can interact with and enhance the warming from other positive feedbacks in the Arctic, such as the SAF.

The result of this is that the warming in the MEBM when the water vapor feedback is locked has a pattern similar to when all feedbacks are included (orange and blue lines in Fig. 3c). A similar point was noted in Langen et al. (2012), who found that when they locked the water vapor feedback in a GCM with doubled CO_2, it produced a pattern of warming that was similar to when the WV feedback was included, but with about half the amplitude. In other words, they found that the WV feedback causes an approximately spatially uniform doubling of the surface temperature response to radiative forcing. Using the MEBM with forcing and feedback fields from individual CMIP5 models, we find that this spatially uniform doubling is a largely robust response among the climate models (Fig. C1 in appendix C).

Next we turn to the lapse rate feedback. In contrast to the water vapor feedback, which is positive everywhere, the lapse rate feedback parameter is negative in the tropical region and positive in the Arctic region (Fig. 1a). This causes the lapse rate feedback to have a large contribution to Arctic amplification in the traditional feedback analysis (Figs. 1c and 2a).

An implication of this for the feedback locking analysis is that the presence of the lapse rate feedback decreases the temperature gradient between the equator and the pole. So when the feedback is locked, the meridional temperature gradient increases, leading to additional transport of MSE into

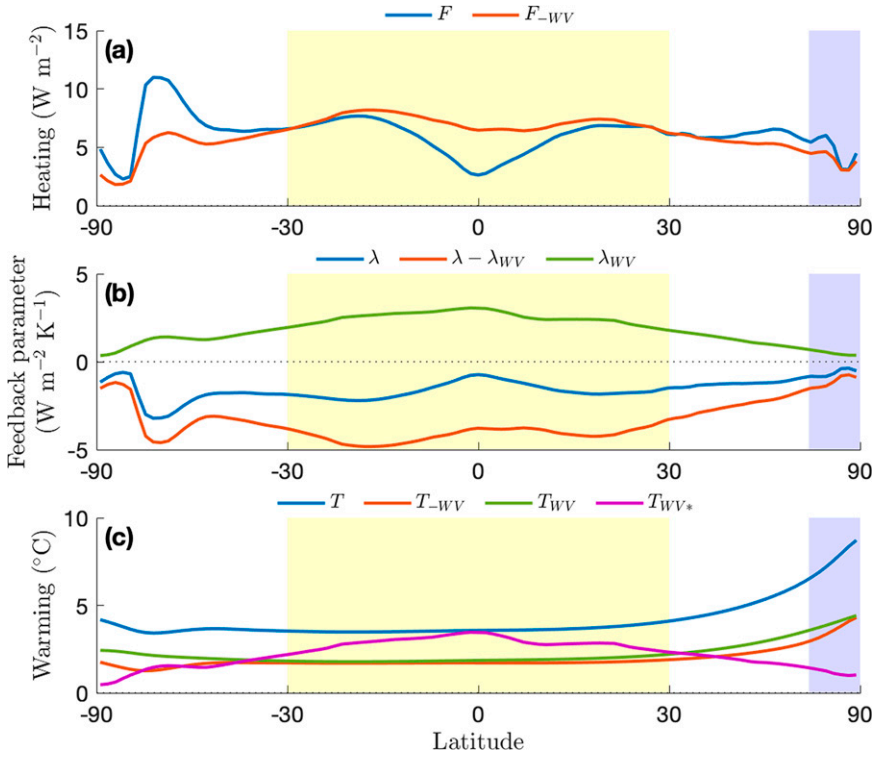

FIG. 3. Feedback locking analysis results for the water vapor feedback. (a) Heating [Eq. (3)] in the MEBM simulation with all feedbacks active (F) and in the MEBM simulation with the water vapor feedback locked ($F_{-\mathrm{WV}}$). Note that all changes in heating are due to changes in AHT, since the perturbation to radiative forcing (F_{RAD}) and ocean heat uptake (F_{OHU}) are specified in the MEBM. (b) Total feedback parameter (λ) and the feedback parameter when the water vapor feedback is locked ($\lambda - \lambda_{\mathrm{WV}}$), with the difference between the two (λ_{WV}) also indicated. (c) Surface temperature change simulated in the MEBM with all feedbacks (T) and with the water vapor feedback locked ($T_{-\mathrm{WV}}$), the warming due to the water vapor feedback based on the feedback locking analysis ($T_{\mathrm{WV}} = T - T_{-\mathrm{WV}}$), and the warming contribution of the water vapor feedback based on the traditional feedback analysis ($T_{\mathrm{WV}*} = T\lambda_{\mathrm{WV}}/-\lambda_0$). Note that the green and purple curves in (c) are equivalent to the red curves in Figs. 1e and 1c, respectively.

the Arctic. (Note that even under uniform warming there would be a relatively small increase in the transport of MSE into the Arctic due to the Clausius–Clapeyron relation; e.g., Merlis and Henry 2018.) This can be seen in Fig. 4a: the inclusion of the lapse rate feedback (going from the red line to the blue line) causes warming in the tropics and cooling in the Arctic due to AHT changes. Hence the AHT changes decrease the level of Arctic amplification, opposing the local feedback effects.

Furthermore, because the lapse rate feedback decreases the level of warming in the tropics, it dampens the effect of other positive feedbacks there, leading to further tropical cooling. Taken together, we find that these effects cause the lapse rate feedback to contribute similar levels of cooling in the tropical and Arctic regions (Figs. 4c and 2b).

The other radiative feedbacks show less dramatic differences between the traditional feedback analysis and the feedback locking analysis (Fig. 2). The differences may be less pronounced because the feedback parameters for the SAF, Planck feedback departure from global mean, and cloud feedbacks do not have such large latitudinal variations between the equator and pole (Fig. 1a). Notably, the surface albedo feedback and Planck feedback anomaly contribute substantially to Arctic amplification in both methods. In other words, they contribute more to Arctic warming than tropical warming due to the feedback pattern alone, and similarly when interactions with other feedbacks and with AHT are included.

4. Decomposition of warming in the feedback locking analysis

The MEBM in Eq. (2) represents an ordinary differential equation for $T(\phi)$ that is nonlinear due to the inclusion of q in F_{AHT}. In the traditional feedback analysis, F_{AHT} is a specified field, so in that case this becomes a linear ordinary differential equation for $T(\phi)$. However, whether or not the terms in Eq. (2) depend linearly on T, there is a nonlinear dependence on λ in the solution for T [as discussed in Roe and

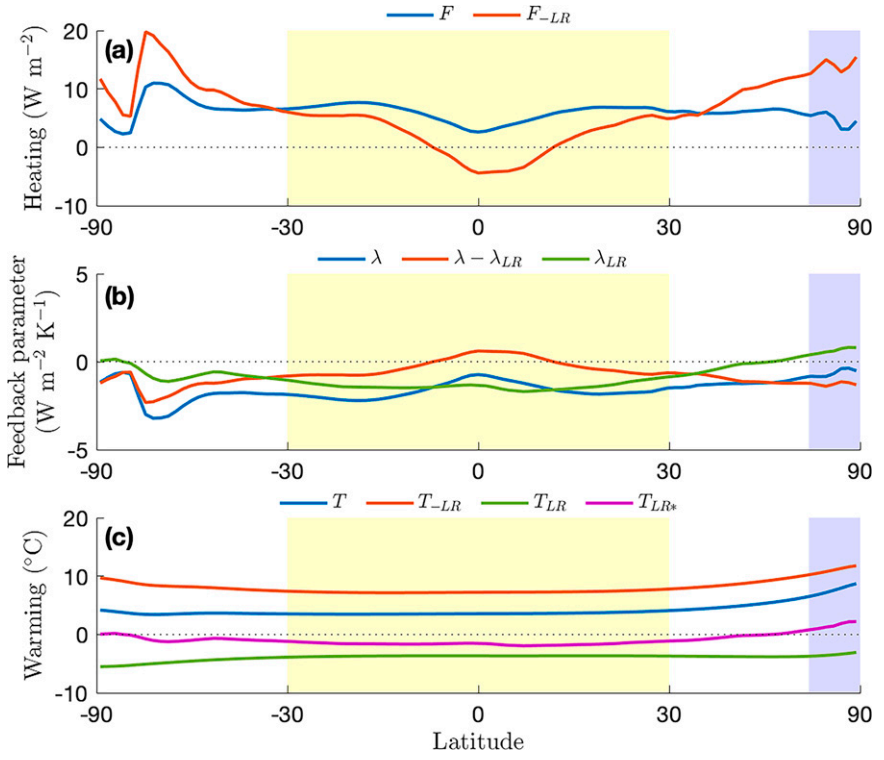

FIG. 4. As in Fig. 3, but for the lapse rate feedback. Note that the green and purple curves in (c) are equivalent to the blue curves in Figs. 1e and 1c, respectively.

Baker (2007)]. Therefore interactions between feedbacks can arise when the inclusion of a feedback changes the total warming T and this, in turn, changes the warming produced by other feedbacks. Since F_{AHT} is computed using the MEBM in each feedback locking simulation, there are also interactions between each feedback and the AHT, in that the AHT adjusts to regional changes in warming induced by each feedback.

Hence the warming attributed to a given feedback process in the feedback locking analysis can be thought of as comprising three separate components: 1) the warming due to the feedback in isolation which is equivalent to the result of the traditional feedback analysis, 2) the warming due to interactions between the feedback and other climate feedbacks, and 3) the warming due to interactions between the feedback and AHT. The contributions of these three terms can be identified by subtracting the equation for the MEBM with a feedback locked (9) from the equation for the full MEBM (2):

$$0 = \lambda T - (\lambda - \lambda_i)T_{-i} + F - F_{-i}, \tag{11}$$

where we have omitted the coordinate ϕ for brevity. Rewriting the total feedback parameter given by Eq. (1) as $\lambda = \lambda_0 + \lambda_i + \sum_{j\neq i}\lambda_j$ and using the definition of T_i in Eq. (10), this can be rewritten as

$$0 = \lambda_0 T_i + \lambda_i T + \sum_{j\neq i}\lambda_j T_i + F - F_{-i}, \tag{12}$$

which can be rearranged to give

$$T_i = \underbrace{T_{i^*}}_{\substack{\text{individual warming}\\ \text{contribution}}} + \underbrace{\frac{\sum_{j\neq i}\lambda_j T_i}{-\lambda_0}}_{\substack{\text{feedback}\\ \text{interactions}}} + \underbrace{\frac{F - F_{-i}}{-\lambda_0}}_{\text{AHT interactions}}. \tag{13}$$

The left-hand side of Eq. (13) is the warming from a feedback process in the feedback locking analysis, and the first term on the right-hand side is the warming contribution from the traditional feedback analysis [Eq. (8)]. The results of the two analyses differ due to the other two terms: the second term on the right-hand side is the product of all other feedback parameters and the warming associated with the inclusion of feedback i (normalized by $-\lambda_0$), and the third term arises from changes in AHT (since F and F_{-i} differ only in their values of F_{AHT}). The values of each of the terms in Eq. (13) for simulations in which each feedback is locked are shown in Fig. 5.

Decomposing the warming due to the water vapor feedback, we find that the interaction between the water vapor feedback and other positive feedbacks in the Arctic is the largest factor contributing to why the water vapor feedback warms the Arctic more than the tropics in the feedback locking analysis, with changes in AHT having a smaller effect (Fig. 5b). For the lapse rate feedback, we find that interactions with other feedbacks leads to cooling in the Arctic that is nearly as large as the tropical cooling from interactions with other feedbacks (Fig. 5a); alongside the changes in AHT, these lead the lapse rate feedback to have a large cooling effect in both regions.

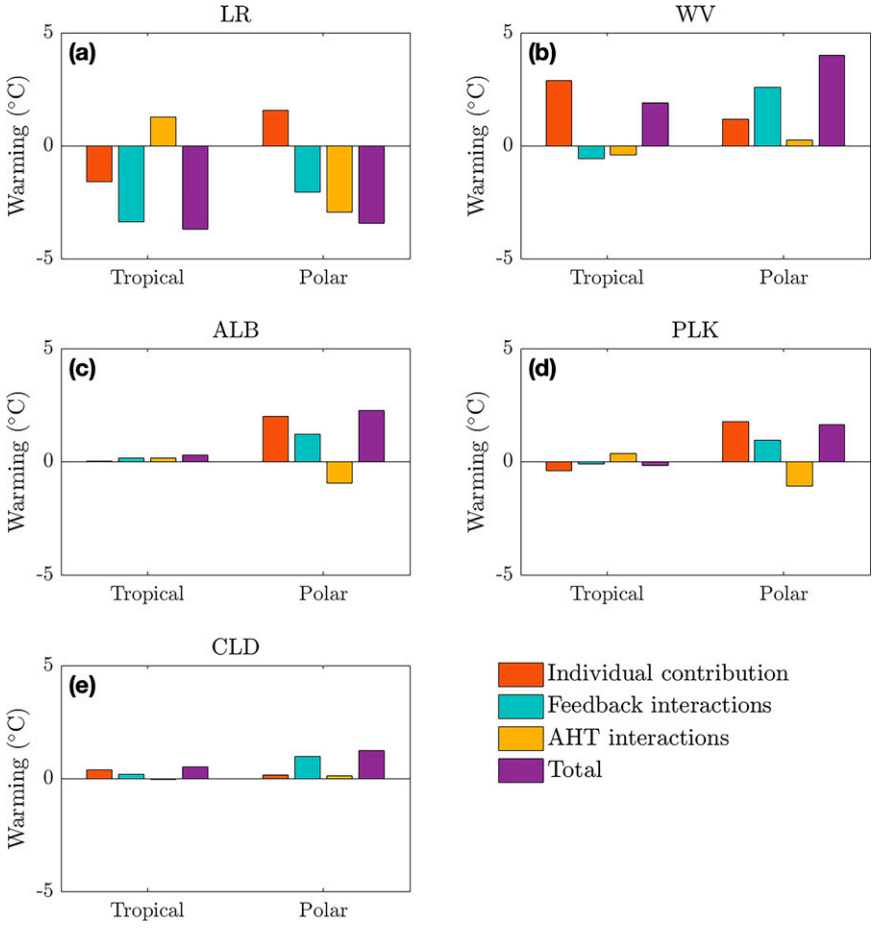

FIG. 5. Decomposition of simulated warming attributed to each feedback using locking simulations (Total) into contributions from the individual contribution of the feedback alone (equivalent to the result from the traditional feedback analysis), interactions with other feedbacks, and interactions with AHT, as described in Eq. (13). Tropical (30°S–30°N) and polar (60°–90°N) values are shown for the warming attributed to the lapse rate feedback (LR), water vapor feedback (WV), surface albedo feedback (ALB), Planck feedback departure from global-mean value (PLK), and cloud feedbacks (CLD).

The decomposition of the simulated warming in Figs. 5c–e also shows that the contributions from changes in AHT and interactions with the other feedbacks are smaller for the warming associated with other feedbacks (surface albedo feedback, deviation from global mean Planck feedback, and cloud feedbacks).

This decomposition illustrates some of the trade-offs between the feedback locking analysis and the traditional feedback analysis. In the traditional feedback analysis, interactions between feedbacks and with AHT, although included, are not easily interpreted, as they are split up among the warming contribution terms. For example, the total warming from feedback interactions that arise from the inclusion of the SAF will not all be included in the SAF warming contribution term using this decomposition [see Eq. (8)]. However, in the traditional feedback analysis the sum of each warming contribution is equal to the total warming, whereas this is not the case when one sums up each of the warming terms found using the feedback locking analysis.

5. Discussion

a. Changes in global-mean surface temperature

Using a traditional feedback analysis to attribute contributions to Arctic amplification is an expansion of the standard climate feedback approach that analyzes the global-mean surface temperature response to a perturbation in the global-mean TOA radiation. However, unlike for the traditional feedback analysis of contributions to Arctic amplification, we find that the global-mean results of a traditional climate feedback analysis and the global-mean results of a feedback locking analysis with the MEBM are monotonically related (see Fig. D1 in appendix D). The relationship between the results from the two types of analysis is not linear due to feedback

interactions, but we find that a feedback locking analysis consistently attributes more warming to feedbacks with larger global feedback parameter values. Hence the results of this study should not be seen as at odds with traditional climate feedback analyses that use global feedback parameter values.

b. Comparison with previous studies

Some previous studies have combined the lapse rate feedback with the water vapor feedback when considering their contributions to warming, motivated by the close physical connection between these feedbacks and their compensatory effects in the tropics. This has been found to diminish the differences in global feedback values diagnosed from different comprehensive climate models (e.g., Soden and Held 2006). An alternative decomposition that can reduce the cancellation between these two feedbacks, as well as the Planck feedback, is to hold the relative humidity fixed in the calculation of the lapse rate and Planck feedbacks and account for changes in relative humidity in a humidity feedback term (Held and Shell 2012; Zelinka et al. 2020; Jeevanjee et al. 2021), rather than the traditional approach in which specific humidity is held fixed in the calculation of the lapse rate and Planck feedbacks and changes in specific humidity are accounted for in the water vapor feedback. It has also been suggested that partitioning the lapse rate feedback into upper and lower atmosphere contributions allows the roles of local and remote driving mechanisms to be more transparently identified (Feldl et al. 2020). Here we instead adopt the classical separation between the lapse rate and water vapor feedbacks because this allows a more direct comparison with previous traditional feedback analyses that also adopted this separation. A message of this study, however, is that the quantification of feedback contributions depends on how feedbacks and contributions are defined, and this needs to be taken into account when comparing studies.

One recent study that also adopted a feedback locking approach is that of Russotto and Biasutti (2020), who investigated how feedbacks contribute to Arctic amplification in a set of idealized slab ocean aquaplanet GCM simulations that did not include sea ice. They found the water vapor feedback to have a positive contribution to Arctic amplification, similar to the present study, but their simulations omitted the SAF, which is a large positive feedback in the Arctic and has substantial interactions with the water vapor feedback in the results presented here.

Note that instead of using the feedback locking approach, which compares simulations using λ and $\lambda - \lambda_i$, an alternative "feedback activation" approach would evaluate the change in temperature response due to activating only a single feedback in a base state with no other feedbacks included (comparing $\lambda_0 + \lambda_i$ with λ_0). In the present study, we adopt the feedback locking approach because we see it as more physically intuitive in that it compares a physically perturbed climate system with the actual climate system. The feedback activation approach does not account for interactions between feedbacks, and neither of the two temperature responses that are compared represents the climate in the presence of all feedbacks.

c. Limitations of the feedback locking analysis

One of the limitations of feedback locking analyses is that the results depend on which other feedbacks and energy transports are included in the model. Consequently, the temperature changes in the MEBM feedback locking simulations are expected to differ somewhat from feedback locking simulations carried out with a comprehensive GCM, which represents more processes and effectively has interactively calculated feedback parameters that can vary with climate. In the MEBM simulations presented here, by contrast, each feedback parameter $[\lambda_i(\phi)]$ remains unchanged when other feedbacks are locked. Although this is expected to be a source of inaccuracy, it has been shown previously that it is a relatively accurate approximation to treat feedback patterns as time invariant over climates ranging from preindustrial to doubled CO_2 (Armour et al. 2013).

Another caveat is that the feedback locking analysis and traditional feedback analysis both approximate the warming by feedbacks to be linearly proportional to the surface temperature change, with variations in the vertical structure of warming captured in the lapse rate feedback. However, it is known that certain feedbacks and heating terms have vertical structures that have implications for Arctic amplification. For example, the water vapor feedback primarily warms the surface in the Arctic, as does the surface albedo feedback (e.g., Screen and Simmonds 2010; Henry et al. 2021). In contrast, poleward heat transport into the Arctic tends to warm the midtroposphere (e.g., Graversen et al. 2008). This could be addressed in further work that uses the feedback locking approach adopted here with a model that more directly accounts for vertical variations. For example, Cai (2006) used a four-box formulation to investigate the changes in the meridional temperature gradient in the atmosphere, and Henry et al. (2021) used a single-column model to study polar amplification. The latter study found that the water vapor feedback has a positive contribution to Arctic amplification due to the warming maximum associated with the water vapor feedback being near the surface in high latitudes but in the upper troposphere in low latitudes. This suggests that adding a representation of vertical variations to the present analysis could plausibly enhance the result that the water vapor feedback contributes to Arctic amplification. On the other hand, Henry and Merlis (2019) found that when linearizing the Stefan–Boltzmann law, polar amplification from the Planck feedback reduced as expected, but this was compensated by an increase in polar amplification from the lapse rate feedback due to the nonlinearity of the Stefan–Boltzmann law changing the vertical structure of warming. Another approach that accounts for vertical variations in the temperature response is the climate feedback-response analysis method (CFRAM) (Lu and Cai 2009; Cai and Lu 2009), which extends the traditional feedback analysis framework to show the 3D warming contribution fields associated with each feedback.

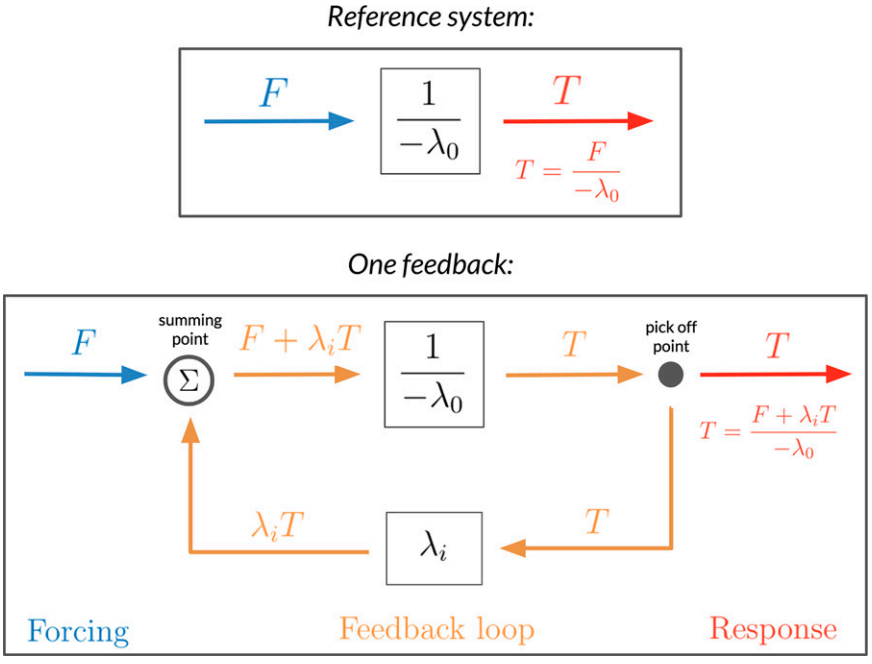

FIG. A1. Schematic of the standard framework for analyzing climate feedbacks, using the analogy to an electrical circuit (cf. Roe 2009 and Goosse et al. 2018). (top) Reference system. (bottom) System that includes one feedback.

d. *Arctic amplification definition*

It should be noted that these results depend both on how Arctic amplification is defined and how the separate feedbacks are defined. In this study, we keep the same definition of feedbacks and Arctic amplification for both methods. We define Arctic amplification as the difference in warming between the Arctic and tropical regions depicted in Fig. 2, which has similarly been used in previous studies (e.g., Pithan and Mauritsen 2014; Goosse et al. 2018; Stuecker et al. 2018). This differs from instead defining Arctic amplification as the Arctic warming divided by the tropical (or global-mean) warming, as adopted in some other studies (e.g., Holland and Bitz 2003; Hwang et al. 2011; Langen et al. 2012). When calculating the level of Arctic amplification using the latter definition, cooling both regions equally has a larger positive effect on Arctic amplification than warming both regions equally, and we find that based on the feedback locking analysis the lapse rate feedback makes a substantial contribution to the ratio definition of Arctic amplification.

6. Summary

Previous studies have used traditional feedback analyses to investigate the contribution of each climate feedback process to the Arctic amplification of global warming. Here we instead adopted a feedback locking approach, in which the warming is computed with an MEBM when each feedback process is turned off. Traditional feedback analyses do not account for each feedback's interactions with the other feedbacks and with AHT, whereas feedback locking analyses do account for these interactions. Feedback locking analyses are also arguably more physically intuitive, in that they assess how much warming would occur in the absence of a given climate feedback process. We find that adopting a feedback locking approach substantially changes the warming attributed to each feedback process.

Specifically, we find that the water vapor feedback is the primary factor contributing to Arctic amplification according to the feedback locking analysis, which is largely due to the water vapor feedback amplifying other positive feedbacks in the Arctic. This is in contrast with previous studies that found the water vapor feedback to be the primary factor opposing Arctic amplification based on traditional feedback analyses. Additionally, we find that the lapse rate feedback has an approximately equivalent contribution to surface cooling in the tropical and Arctic regions in a feedback locking analysis, whereas previous studies found it to be the main driver of Arctic amplification according to traditional feedback analyses. This suggests, for example, that an idealized model that omits a representation of the water vapor feedback would do a worse job of capturing Arctic amplification than an idealized model that omits a representation of the lapse rate feedback, in contrast with expectations based on previous studies that relied on traditional feedback analyses. Overall, these results highlight that determining which feedbacks are most important for Arctic amplification depends crucially on what approach is used to determine the contribution of each feedback process.

Acknowledgments. Many thanks to Kyle Armour for providing the MEBM code, Dave Bonan for helping with the MEBM code and for comments on the manuscript, Tim Merlis for comments on the manuscript and for suggestions that led to the analysis in Fig. C1, and Isaac Held and Nadir Jeevanjee for helpful discussions and comments on the manuscript. This work was supported by National Science Foundation Grant OPP-1643445.

Data availability statement. The CMIP5 data used in this study are accessible at the Earth System Grid Federation (ESGF) Portal (https://esgf-node.llnl.gov/search/cmip5/).

APPENDIX A

Traditional Climate Feedback Analysis Framework

The standard framework for analyzing climate feedbacks is illustrated in Fig. A1, using a schematic analogy to an electrical circuit. A perturbation to the forcing (F) is sent through a reference system, which is taken here as the negative inverse of the global-mean Planck feedback parameter (λ_0, which is typically in units of W m^{-2} K^{-1}), resulting in a change in surface temperature (T) to maintain radiative balance. A feedback is incorporated into the system by taking the response at the "pick off point" and sending it through an additional perturbation to the radiative forcing due to the feedback (λ_i) and then bringing it to the "summing point." The total perturbation to the radiative forcing is then sent through the reference system.

TABLE B1. Sources of parameters and variables.

Variable	Output from MEBM	Calculated using TOA budget analysis	Calculated using radiative kernels
F_{RAD}		×	
F_{OHU}		×	
λ		×	
λ_i			×
F_{AHT}	×		
T	×		

APPENDIX B

Spatially Varying Fields in the MEBM

The MEBM parameters for spatially varying feedbacks and heating fields are taken from CMIP5 output, as described by Bonan et al. (2018) and briefly summarized here (Table B1). Zonal-mean TOA budget analyses are used to calculate F_{RAD}, F_{OHU}, and λ: F_{RAD} is calculated as the change in TOA radiation in fixed sea surface temperature simulations under CO_2 quadrupling, F_{OHU} is calculated as the change in net surface heat flux in CMIP5 coupled GCM abrupt CO_2 quadrupling simulations averaged over years 85–115, and λ is calculated by equating the TOA net radiation anomaly with $\lambda T + F_{\mathrm{RAD}}$ in the same CMIP5 coupled GCM output.

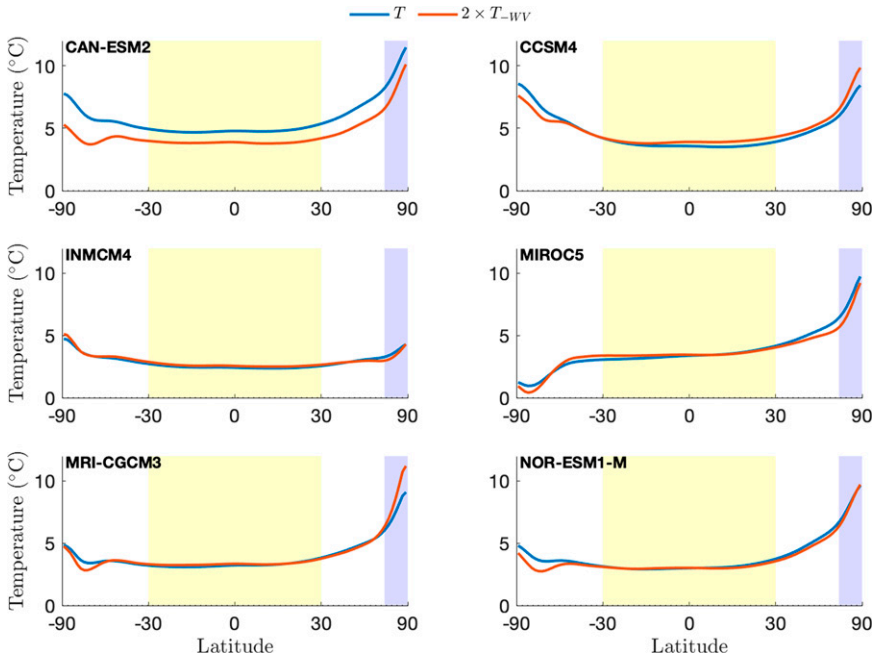

FIG. C1. Water vapor feedback climate sensitivity in individual CMIP5 models. Change in surface temperature in the MEBM with all feedbacks (blue) and twice the change in surface temperature with the water vapor feedback locked (orange) for six CMIP5 models (name in bold) are plotted. The similarity of the blue and orange lines suggest that water vapor approximately doubles climate sensitivity.

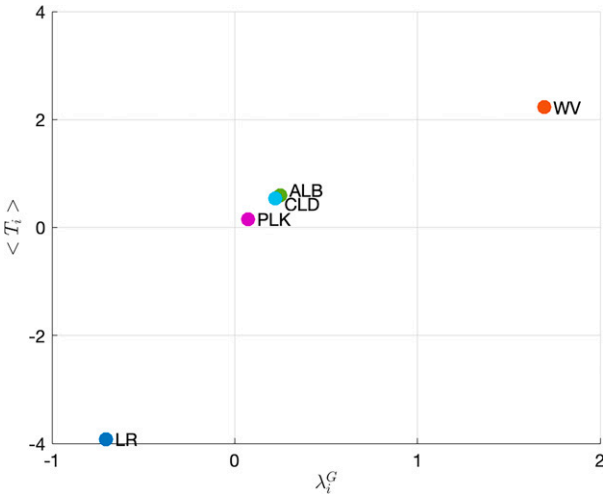

FIG. D1. Global-mean surface warming calculated from locking simulations compared with the global feedback parameter (λ_i^G) for each radiative feedback. Feedbacks are labeled as in Fig. 5. In this global-mean analysis, the contribution of each feedback using locking simulations in the MEBM scales monotonically with the global feedback parameter.

Radiative kernels are used to partition λ into individual feedbacks parameters λ_i; note that the radiative kernel analysis uses a somewhat different set of CMIP5 GCMs than the TOA budget analysis, as described by Bonan et al. (2018) (Table 1 of their supporting information, with the exception that models FGOALS-S2 and HADGEM2-ES are not used in our calculations of F_{RAD}, F_{OHU}, and λ). Throughout the present analysis, we use values of F_{AHT} and T that are simulated by the MEBM.

APPENDIX C

Comparing the Local Climate Sensitivity of the Water Vapor Feedback in Individual Models

The water vapor feedback approximately doubles the climate sensitivity at each location, meaning that the warming field in the MEBM without the water vapor feedback is approximately equal to the warming field in the MEBM with all feedbacks scaled by one-half. This is shown for individual CMIP5 models in Fig. C1.

APPENDIX D

Traditional Feedback Analysis versus Feedback Locking for Global-Mean Temperature Changes

The traditional feedback analysis is based on analyses used to look at the contributions from individual feedbacks to global-mean surface temperature changes. Here we compare the warming contributions from a feedback analysis with the results of feedback locking for the global-mean temperature. Beginning with the former, the global average of Eq. (2) is

$$0 = \langle \lambda T \rangle + \langle F \rangle, \tag{D1}$$

where angle brackets indicate the global-mean value. We define the global feedback parameter value λ_i^G of each individual feedback as

$$\lambda_i^G \equiv \frac{\langle \lambda_i T \rangle}{\langle T \rangle}. \tag{D2}$$

Inserting Eq. (1) into Eq. (D1) and rearranging gives

$$\langle T \rangle = \frac{\langle F \rangle}{-\lambda_0} + \sum_i \lambda_i^G \frac{\langle T \rangle}{-\lambda_0}, \tag{D3}$$

which is the global-mean equivalent of Eq. (7), with the warming contributions from each feedback given here as

$$\langle T_{i*} \rangle \equiv \lambda_i^G \frac{\langle T \rangle}{-\lambda_0}. \tag{D4}$$

Hence since λ_0 and $\langle T \rangle$ are globally constant, the global warming contribution for each feedback scales with the global feedback parameter value λ_i^G. We can compare this with the global-mean warming calculated from the locking simulations in the MEBM, given by the global-mean equivalent of Eq. (10), which is $\langle T_i \rangle \equiv \langle T \rangle - \langle T_{-i} \rangle$. The levels of warming attributed to each feedback using the two approaches are plotted in Fig. D1.

REFERENCES

Alexeev, V. A., and C. H. Jackson, 2013: Polar amplification: Is atmospheric heat transport important? *Climate Dyn.*, **41**, 533–547, https://doi.org/10.1007/s00382-012-1601-z.

——, P. L. Langen, and J. R. Bates, 2005: Polar amplification of surface warming on an aquaplanet in "ghost forcing" experiments without sea ice feedbacks. *Climate Dyn.*, **24**, 655–666, https://doi.org/10.1007/s00382-005-0018-3.

Armour, K. C., C. M. Bitz, and G. H. Roe, 2013: Time-varying climate sensitivity from regional feedbacks. *J. Climate*, **26**, 4518–4534, https://doi.org/10.1175/JCLI-D-12-00544.1.

——, N. Siler, A. Donohoe, and G. H. Roe, 2019: Meridional atmospheric heat transport constrained by energetics and mediated by large-scale diffusion. *J. Climate*, **32**, 3655–3680, https://doi.org/10.1175/JCLI-D-18-0563.1.

Beer, E., I. Eisenman, and T. J. W. Wagner, 2020: Polar amplification due to enhanced heat flux across the halocline. *Geophys. Res. Lett.*, **47**, e2019GL086706, https://doi.org/10.1029/2019GL086706.

Bonan, D. B., K. C. Armour, G. H. Roe, N. Siler, and N. Feldl, 2018: Sources of uncertainty in the meridional pattern of climate change. *Geophys. Res. Lett.*, **45**, 9131–9140, https://doi.org/10.1029/2018GL079429.

Budyko, M., 1969: Effect of solar radiation variations on climate of Earth. *Tellus*, **21**, 611–619, https://doi.org/10.3402/tellusa.v21i5.10109.

Cai, M., 2006: Dynamical greenhouse-plus feedback and polar warming amplification. Part I: A dry radiative-transportive climate model. *Climate Dyn.*, **26**, 661–675, https://doi.org/10.1007/s00382-005-0104-6.

——, and J. Lu, 2009: A new framework for isolating individual feedback processes in coupled general circulation climate models. Part II: Method demonstrations and comparisons.

Climate Dyn., **32**, 887–900, https://doi.org/10.1007/s00382-008-0424-4.

Cess, R., and Coauthors, 1991: Interpretation of snow–climate feedback as produced by 17 general circulation models. *Science*, **253**, 888–892, https://doi.org/10.1126/science.253.5022.888.

Collins, M., and Coauthors, 2013: Long-term climate change: Projections, commitments and irreversibility. *Climate Change 2013: The Physical Science Basis*, T. F. Stocker et al., Eds., Cambridge University Press, 1029–1136, https://doi.org/10.1017/CBO9781107415324.024.

Dee, D. P., and Coauthors, 2011: The ERA-Interim reanalysis: Configuration and performance of the data assimilation system. *Quart. J. Roy. Meteor. Soc.*, **137**, 553–597, https://doi.org/10.1002/qj.828.

Dufresne, J.-L., and S. Bony, 2008: An assessment of the primary sources of spread of global warming estimates from coupled atmosphere–ocean models. *J. Climate*, **21**, 5135–5144, https://doi.org/10.1175/2008JCLI2239.1.

Feldl, N., S. Po-Chedley, H. K. A. Singh, S. Hay, and P. J. Kushner, 2020: Sea ice and atmospheric circulation shape the high-latitude lapse rate feedback. *npj Climate Atmos. Sci.*, **3**, 41, https://doi.org/10.1038/s41612-020-00146-7.

Francis, J. A., and E. Hunter, 2006: New insight into the disappearing Arctic sea ice. *Eos, Trans. Amer. Geophys. Union*, **87**, 509–511, https://doi.org/10.1029/2006EO460001.

Goosse, H., and Coauthors, 2018: Quantifying climate feedbacks in polar regions. *Nat. Commun.*, **9**, 1919, https://doi.org/10.1038/s41467-018-04173-0.

Graversen, R. G., and M. Wang, 2009: Polar amplification in a coupled climate model with locked albedo. *Climate Dyn.*, **33**, 629–643, https://doi.org/10.1007/s00382-009-0535-6.

——, T. Mauritsen, M. Tjernstrom, E. Kallen, and G. Svensson, 2008: Vertical structure of recent Arctic warming. *Nature*, **451**, 53–56, https://doi.org/10.1038/nature06502.

Hall, A., 2004: The role of surface albedo feedback in climate. *J. Climate*, **17**, 1550–1568, https://doi.org/10.1175/1520-0442(2004)017<1550:TROSAF>2.0.CO;2.

Held, I. M., and K. M. Shell, 2012: Using relative humidity as a state variable in climate feedback analysis. *J. Climate*, **25**, 2578–2582, https://doi.org/10.1175/JCLI-D-11-00721.1.

Henry, M., and T. M. Merlis, 2019: The role of the nonlinearity of the Stefan-Boltzmann law on the structure of radiatively forced temperature change. *J. Climate*, **32**, 335–348, https://doi.org/10.1175/JCLI-D-17-0603.1.

——, ——, N. J. Lutsko, and B. E. J. Rose, 2021: Decomposing the drivers of polar amplification with a single-column model. *J. Climate*, **34**, 2355–2365, https://doi.org/10.1175/JCLI-D-20-0178.1.

Holland, M., and C. Bitz, 2003: Polar amplification of climate change in coupled models. *Climate Dyn.*, **21**, 221–232, https://doi.org/10.1007/s00382-003-0332-6.

Hwang, Y.-T., and D. M. W. Frierson, 2010: Increasing atmospheric poleward energy transport with global warming. *Geophys. Res. Lett.*, **37**, L24807, https://doi.org/10.1029/2010GL045440.

——, ——, and J. E. Kay, 2011: Coupling between Arctic feedbacks and changes in poleward energy transport. *Geophys. Res. Lett.*, **38**, L17704, https://doi.org/10.1029/2011GL048546.

Jeevanjee, N., D. D. B. Koll, and N. Lutsko, 2021: "Simpson's law" and the spectral cancellation of climate feedbacks. *Geophys. Res. Lett.*, **48**, e2021GL093699, https://doi.org/10.1029/2021GL093699.

Kay, J. E., and A. Gettelman, 2009: Cloud influence on and response to seasonal Arctic sea ice loss. *J. Geophys. Res.*, **114**, D18204, https://doi.org/10.1029/2009JD011773.

Langen, P. L., R. G. Graversen, and T. Mauritsen, 2012: Separation of contributions from radiative feedbacks to polar amplification on an aquaplanet. *J. Climate*, **25**, 3010–3024, https://doi.org/10.1175/JCLI-D-11-00246.1.

Lu, J., and M. Cai, 2009: A new framework for isolating individual feedback processes in coupled general circulation climate models. Part I: Formulation. *Climate Dyn.*, **32**, 873–885, https://doi.org/10.1007/s00382-008-0425-3.

Mahlstein, I., and R. Knutti, 2011: Ocean heat transport as a cause for model uncertainty in projected Arctic warming. *J. Climate*, **24**, 1451–1460, https://doi.org/10.1175/2010JCLI3713.1.

Merlis, T. M., 2014: Interacting components of the top-of-atmosphere energy balance affect changes in regional surface temperature. *Geophys. Res. Lett.*, **41**, 7291–7297, https://doi.org/10.1002/2014GL061700.

——, and M. Henry, 2018: Simple estimates of polar amplification in moist diffusive energy balance models. *J. Climate*, **31**, 5811–5824, https://doi.org/10.1175/JCLI-D-17-0578.1.

Middlemas, E. A., J. E. Kay, B. M. Medeiros, and E. A. Maroon, 2020: Quantifying the influence of cloud radiative feedbacks on Arctic surface warming using cloud locking in an Earth system model. *Geophys. Res. Lett.*, **47**, e2020GL089207, https://doi.org/10.1029/2020GL089207.

Myhre, G., and Coauthors, 2013: Anthropogenic and natural radiative forcing. *Climate Change 2013: The Physical Science Basis*, T. F. Stocker et al., Eds., Cambridge University Press, 659–740.

Pithan, F., and T. Mauritsen, 2014: Arctic amplification dominated by temperature feedbacks in contemporary climate models. *Nat. Geosci.*, **7**, 181–184, https://doi.org/10.1038/ngeo2071.

Roe, G. H., 2009: Feedbacks, timescales, and seeing red. *Annu. Rev. Earth Planet. Sci.*, **37**, 93–115, https://doi.org/10.1146/annurev.earth.061008.134734.

——, and M. B. Baker, 2007: Why is climate sensitivity so unpredictable? *Science*, **318**, 629–632, https://doi.org/10.1126/science.1144735.

——, N. Feldl, K. C. Armour, Y.-T. Hwang, and D. M. W. Frierson, 2015: The remote impacts of climate feedbacks on regional climate predictability. *Nat. Geosci.*, **8**, 135–139, https://doi.org/10.1038/ngeo2346.

Rose, B. E. J., K. C. Armour, D. S. Battisti, N. Feldl, and D. D. B. Koll, 2014: The dependence of transient climate sensitivity and radiative feedbacks on the spatial pattern of ocean heat uptake. *Geophys. Res. Lett.*, **41**, 1071–1078, https://doi.org/10.1002/2013GL058955.

Russotto, R. D., and M. Biasutti, 2020: Polar amplification as an inherent response of a circulating atmosphere: Results from the TRACMIP aquaplanets. *Geophys. Res. Lett.*, **47**, e2019GL08, https://doi.org/10.1029/2019GL086771.

Screen, J. A., and I. Simmonds, 2010: The central role of diminishing sea ice in recent Arctic temperature amplification. *Nature*, **464**, 1334–1337, https://doi.org/10.1038/nature09051.

Sellers, W. D., 1969: A global climatic model based on the energy balance of the Earth–atmosphere system. *J. Appl. Meteor.*, **8**, 392–400, https://doi.org/10.1175/1520-0450(1969)008<0392:AGCMBO>2.0.CO;2.

Siler, N., G. H. Roe, and K. C. Armour, 2018: Insights into the zonal-mean response of the hydrologic cycle to global warming from a diffusive energy balance model. *J. Climate*, **31**, 7481–7493, https://doi.org/10.1175/JCLI-D-18-0081.1.

Soden, B. J., and I. M. Held, 2006: An assessment of climate feedbacks in coupled ocean–atmosphere models. *J. Climate*, **19**, 3354–3360, https://doi.org/10.1175/JCLI3799.1; Corrigendum, **19**, 6263, https://doi.org/10.1175/JCLI9028.1.

Stuecker, M. F., and Coauthors, 2018: Polar amplification dominated by local forcing and feedbacks. *Nat. Climate Change*, **8**, 1076+, https://doi.org/10.1038/s41558-018-0339-y.

Taylor, K. E., R. J. Stouffer, and G. A. Meehl, 2012: An overview of CMIP5 and the experiment design. *Bull. Amer. Meteor. Soc.*, **93**, 485–498, https://doi.org/10.1175/BAMS-D-11-00094.1.

Taylor, P. C., M. Cai, A. Hu, G. A. Meehl, W. Washington, and G. J. Zhang, 2013: A decomposition of feedback contributions to polar warming amplification. *J. Climate*, **26**, 7023–7043, https://doi.org/10.1175/JCLI-D-12-00696.1; Corrigendum, **26**, 8706, https://doi.org/10.1175/JCLI-D-13-00511.1.

Zelinka, M. D., T. A. Myers, D. T. McCoy, S. Po-Chedley, P. M. Caldwell, P. Ceppi, S. A. Klein, and K. E. Taylor, 2020: Causes of higher climate sensitivity in CMIP6 models. *Geophys. Res. Lett.*, **47**, e2019GL085782, https://doi.org/10.1029/2019GL085782.